

## THE EFFECT OF WAVEGUIDE MATERIAL AND SHAPE ON AE TRANSMISSION CHARACTERISTICS

**Joanna Sikorska**  
**Jie Pan**

University of Western Australia  
Perth, Australia

### ABSTRACT:

Acoustic emission testing (AET) often utilises waveguides to separate delicate sensors from hot surfaces or to facilitate access to otherwise obstructed materials such as lagged vessels. In the authors' work, restricted access to mechanical seals on a hot water pump necessitated the use of a short rod to transmit acoustic emission (AE) information from the ceramic seal face. Consequently, an appreciation was required of how this waveguide altered the seal's AE signals.

This paper presents the effects of varying the material and/or shape on the temporal and frequency characteristics of pulsed acoustic emission events travelling through small cylindrical rods. 36 waveguides, fabricated from either alumina ceramic, mild steel, stainless steel (SS316) or extruded Delrin were tested, of 3 different lengths, two diameters and four sensor face angles. The effect of a point at the source end of the waveguide was also verified.

### 1 RELEVANT ULTRASONIC THEORY

The solutions to the general wave equation for acoustic waves travelling through isotropic cylinders are detailed in references [1]-[3]. However, there are several key points applicable to this research work that will now be summarised.

Longitudinal (i.e. compressional) wave modes in a cylinder vary with radial and longitudinal distance along the cylinder but are symmetrical around the circumference. The relationship between phase velocity and frequency is known as the Pochhammer-Chree equation and resembles the Lamb dispersion relationship in plates. From this equation, it can be seen that the fundamental mode approaches a constant velocity as  $ka$  approaches zero, where  $k$  is the wavenumber and  $a$  is the cylinder radius. This limiting velocity corresponds to the longitudinal rod velocity:

$$c_L = \sqrt{\frac{E}{\rho}} \quad (1.1)$$

where  $E$  is the Young's modulus for the material and  $\rho$  is the density. As  $ka$  increases (i.e. frequency increases) to a value between 1 and 2, the first longitudinal mode asymptotes to the Rayleigh velocity. Rayleigh waves are surface acoustic waves in which longitudinal and shear modes couple together and travel at a common velocity; it is always less than the transverse velocity by 5 to 15% [4]. They also decay rapidly with depth and therefore displacements are confined to within one order of Rayleigh wavelengths from the surface. Rayleigh waves are the primary means by which high frequency longitudinal signals are transmitted across significant distances.

Higher longitudinal modes have cut-off frequencies below which they will not propagate, and above which they are dispersive.

Torsional waves also propagate with one constant velocity fundamental mode equal to the shear (or transverse) velocity:

$$c_T = \sqrt{\frac{E}{\rho} \cdot \frac{1}{2(1+\nu)}} \quad (1.2)$$

where  $\nu$  is the Poisson's ratio. Again, higher modes are dispersive and each has a unique cut-off frequency below which these modes will not propagate. If the distance from the source is sufficient, cut-off effects act like a high pass filter, leaving only the primary modes as the means by which low frequency longitudinal and transverse waves can be transmitted. Conversely, above a certain frequency (below a certain wavenumber) dispersion will no longer occur as speeds approach their limiting velocity. Similar, but mathematically more complex relationships govern the dispersive characteristics of flexural waves in rods.

An acoustic emission burst however, is made up of numerous waves of different polarizations and consequently, different speeds. Each component will be attenuated, dispersed or reflected differently. Therefore wave speed is typically referred to in terms of group velocity,  $c_g$ . All group modes are dispersive and a single mode may have several different branches (of different frequencies) in existence at any one time. These branches commence and terminate at set times (with respect to pulse initiation) depending on the material properties ( $E, \rho, \nu$ ), rod dimensions ( $a, l$ ) and mode of propagation [1].

In addition to dispersion, other changes affecting travel of AE bursts through a waveguide include mode conversion and attenuation. Acoustic waves are partially reflected and transmitted at every interface, the relative amounts of which depend on the ratio of the relative characteristic impedances of each pair of boundary materials. This impedance is a function of material density and the velocity wave hitting the interface. For non-zero angles of incidence, the character of the wavefront will change as it hits the interface. Called *mode conversion*, the change in angle of the wavefront will convert part of the incoming wave from longitudinal to shear and vice versa. Therefore, acoustic emissions reaching a sensor will inevitably contain both types of waves, irrespective of their original polarization. In fact, the transient waveform will lengthen in time as it moves through a complex bounded medium, due the continuous transformation between modes travelling at different velocities [4].

Some of these modes will not be detectable to the sensor, causing apparent signal attenuation. Energy is also lost to friction and thermal conductivity. Depending on the frequency of the wavefront, attenuation is also affected by the crystalline structure of the material, particularly in compounds with larger grain sizes, such as plastics or composites where this type of energy loss can be up to 3 orders of magnitude greater than in metals. Attenuation is also generally greater for transverse waves than for longitudinal modes.

Rayleigh waves will also lose energy to the surrounding fluid. The significance of this loss is proportional to the relative (fluid to solid) acoustic impedances and inversely proportional to the Rayleigh acoustic wavelength.

## 2 EXPERIMENTAL METHOD

A variety of short waveguides were tested to illustrate the effects of (a) material properties; (b) length; (c) diameter; (d) face angle and (e) source point on the transmission and reception of pulsed AE bursts.

36 waveguides were tested in total, fabricated from four materials: Delrin acetal resin (white extruded bar, exact grade unknown), mild steel (grade unknown), SS316 and sintered 99.9% alumina ceramic ( $\alpha$ -Al<sub>2</sub>O<sub>3</sub>). Approximate material properties are summarised in table 1. Sensor face angles were 0, 30, 45 or 60 degrees; lengths were 30, 43 or 51mm; and diameters were 5 or 8mm. Unless otherwise stated, the rod face attached to the pulser was flat.

Test specimens were grouped as follows:

- (a) 4 sets of 8mm diameter waveguides with face angles of 0, 30, 45 and 60 degrees from each of the four materials (16 waveguides in total). Lengths were set at 43 mm between centres (at which pulser and receiver were located).
- (b) 2 sets of 8mm diameter, shorter (30mm) waveguides with face angles of 0, 30, 45 and 60 degrees from Delrin and SS316.
- (c) 2 sets of narrower (5mm) mild steel rods, 30mm and 43mm in length, with face angles of 0, 30, 45 and 60 degrees.
- (d) 2 longer (51mm) rods from Delrin and SS316, 0 degrees sensor face angle.
- (e) 2 8mm diameter, 43mm long rods from mild steel and SS316 with the pulser face tapered (45 degrees) to a point. The other end was set at 0 degrees. SS316 sample had a sharper point than the mild steel rod.

To quantify the effect of each waveguide, data was also collected from the sensor mounted directly on the pulser face.

Longitudinal pulses representative of AE bursts were generated by a DECI Model SE25-P sensor driven by a DECI Model 600 pulser, set at 150V. A waveguide holder (Figure 1) was fabricated to ensure that the relative positions of the sensor, waveguide and pulser were kept constant. The pulser was attached to the underside of the holder with a Delrin collar containing 8 rare earth magnets and two locating pins to ensure its orientation was identical for every test. Incorporated into the sensor mount was a screw and spring that held the sensor firmly against the top waveguide face. This could be oriented to any angle. O-rings prevented the waveguides from contacting the sides of the sample holder. Silicone grease was used as a couplant between the pulser-waveguide and waveguide-sensor faces.

**Table 1:** Approximate Acoustic Properties of Test Materials

\* Properties given for Delrin 100.

| Material                         | Density<br>(g/cm <sup>3</sup> ) | c <sub>L</sub><br>(mm/μs) | Z <sub>L</sub> | λ <sub>L</sub> @ 20kHz<br>(mm) | λ <sub>L</sub> @ 2MHz<br>(mm) |
|----------------------------------|---------------------------------|---------------------------|----------------|--------------------------------|-------------------------------|
| Delrin *                         | 1.42                            | 1.4                       | 3.45           | 121.5                          | 1.22                          |
| Mild Steel                       | 7.80                            | 5.1                       | 46             | 295                            | 2.95                          |
| SS316                            | 7.89                            | 4.9                       | 45.7           | 289.5                          | 2.9                           |
| α-Al <sub>2</sub> O <sub>3</sub> | 3.86                            | 9.9                       | 40.6           | 526                            | 5.26                          |

Bursts were detected using a B1080 Digital Wavecorp single ended wideband AE sensor connected to a PAC 2/4/6 preamplifier supplying a gain of 20dB and fitted with 100-1000kHz bandpass filters. Data was recorded with a PACNDT PCI2 AE card, which was housed in Pentium IV 2.8GHz Intel desktop computer. Prior to digitisation, signals were bandpass filtered onboard at 1-3000kHz. A fixed trigger threshold was set at 50dB<sub>AE</sub>. For each waveguide, between 128 and 300 triggered waveforms, each consisting of 8192 samples with 256 pre-trigger samples, were collected and digitised at 10MHz.

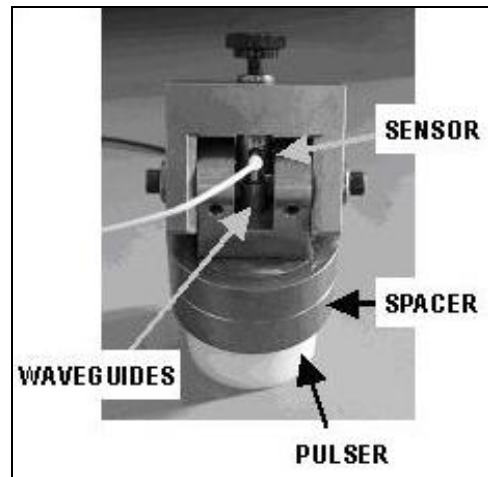


Figure 1: Waveguide holder

Various burst features were collected by PAC's driver software (AEWin) for each triggered event, including amplitude (in dB<sub>AE</sub>), energy, duration, rise time and counts.

### 2.1 Additional Post-processing

32 sequential bursts were then synchronously time-averaged and an averaged FFT also performed by programs written in LabVIEW™ 6.1. Due to the highly transient nature of the AE data, no window or overlapping was applied; as bursts were always captured completely within each dataset, spectral leakage was not considered to be an issue. When multiple files were collected, averaged results are presented.

To exclude the effect of sensor-pulser response, cross-spectra were performed against the face to face averaged signal and results determined in terms of the magnitude and phase output. Coherence was checked, but always found to be equal to one.

Using standard routines within the LabVIEW™ signal processing toolset, a STFT (Short-time-Fourier-Transform) was performed on the averaged bursts to identify individual modes of propagation. The STFT was undertaken using 1024 frequency increments and a Hanning window. As the simultaneous time-frequency resolution of the STFT has functional limitations, two sets of graphs were obtained with time increments of 128 or 512 samples per time window to extract improve temporal and spatial resolution respectively. More details on the STFT algorithms used are available in [6].

## 3 RESULTS AND OBSERVATIONS

*Notes on interpreting graphs:*

The following designation is used to describe samples:

*Material x Diameter in mm x Nominal Length in mm "PT" (optional)*

Abbreviations include:

|  |             |
|--|-------------|
| FF – Face to face (i.e. no waveguide)                  |             |
| PT – Point on pulser end of waveguide (otherwise flat) |             |
| MS – Mild steel  | SS – SS316  |
| AL – $\alpha$ AL <sub>2</sub> O <sub>3</sub>           | DR – Delrin |

Due to the normalisation of bursts prior to applying the STFT, amplitudes on intensity plots only show the relative amplitudes between modes and should not be used to compare waveguides. Frequency and time scales however, are identical.

### 3.1 Burst information

As predicted by the theory overall attenuation of both energy and peak amplitude was greatest in non-metallic waveguides (Figure 3). Attenuation also increased with length (SS, DR and MS), diameter (MS only) and face angle (all four materials) particularly above 30 degrees (Figure 4).

Durations and counts were substantially higher in both grades of steel rods due to a significant number of reflections (Figure 2a); both features increased with rod length. A much larger than expected duration for Face-to-Face bursts (or visually apparent, see Figure 6) is due to the signal decaying from 112dBAE to just above the 50dBAE threshold level within 100 $\mu$ s, but then taking significantly longer to drop below the threshold level. Duration values for waveguide samples however, seem to be accurate representations of their waveform profiles.

Rise times (Figure 2b) were greatest for Delrin, due to its much lower velocity, and for the pointed steel samples, probably due to excessive attenuation of the higher frequency mode branches. Interestingly, the 30mm SS316 samples also had greater rise times than the 43mm SS316 samples and the reason for this is not obvious.

Little difference in the time domain can be seen between mild steel and stainless steel waveguide responses, especially when compared to the non-metallic samples. Frequency spectra (Figure 5) and STFT plots were also very similar.

Pointed 43mm waveguides attenuated the signals by over 12dB when compared to similar flat waveguides with adequate couplant. This was greater than the attenuation quoted in [7]. A sharper point on the SS316 waveguide attenuated the signals more than a blunter point on the MS waveguide and may allude to the discrepancy between these and other published figures. Also, the sharper-pointed SS316 sample appeared less able to transmit various high and low frequency modes, deduced by the absence of these frequencies from the STFT plot (Figure 8).

### 3.2 Modal information

As the exact group velocity dispersion curves were not calculated, it was not possible to conclude with certainty which modes were being excited in each waveguide. However, it is surmised that in all cases the first two longitudinal modes were excited by the pulsations, giving rise to up to five frequencies in the range of interest (100-625 kHz – the presence of any higher frequencies were too small to be seen in the STFT plots). In some cases, higher order modes can also be seen, but these are generally very small when compared to the lower modes. No significant changes in spectral information were observed in STFT plots for angled waveguides; thus it is concluded that if torsional modes were present, their amplitudes were too small, and/or material attenuation too great, for these to be identifiable.

Not surprisingly, Delrin rods displayed the greatest mode separation of all waveguides tested. As predicted, separation increased with waveguide length (Figure 7a). A similar phenomenon was observed in SS waveguides (Figure 7b), although the increased number of reflections in the latter case made identifying the slower modes more difficult from the burst waveforms.

8x43mm Mild Steel and SS316 waveguides (and also SS316 51mm rods) suffered from significant mode conversion and wave reflection. Due to the lack of attenuation these reflections overlapped, thereby complicating mode and original burst identification, as well as increasing signal durations. Frequency spectra were also dominated by resulting harmonics (Figure 5). Mode conversion increased with face angle (Figure 8). The numbers of reflections were smaller in 30-degree samples of both steels, at the expense of some higher frequency information.

Narrower and shorter 5x30mm MS rods did not seem to suffer from mode conversion, or from as many reflections as the wider, longer MS or SS samples. Higher frequency content also reduced; STFT plots were dominated by one non-terminating mode. Further attenuation of any remaining high frequency information occurred in samples with non-zero face angles. Mode conversion and reflection were also evident in the 8x30mm SS samples for all face angles, but again these were fewer and less significant than in the longer samples.

Reflections could also be identified in AL rods. However, due to its higher attenuation reflections did not overlap significantly, facilitating easy identification of the primary burst. Although a number of modes were identified in the STFT plots of AL rods, insufficient resolution was available to identify any differences in arrival times. Appreciable mode conversion could not be observed in any AL samples, irrespective of face angle. Conversely, the STFT plot for the 60-degree AL rod comprised of only two discernible frequencies, with almost all energy contained in one non-terminating mode.

#### 4 CONCLUSIONS

Although signals were attenuated less by mild steel and SS316 waveguides, resonance artefacts dominated frequency responses in longer and/or wider rods. Of these, only the set of 5x30mm mild steel waveguides appeared free of reflections or mode conversion, indicating that these conditions were amplified by increasing waveguide diameter and/or length. It is possible that much longer waveguides (>100mm) might avoid this problem due to the additional attenuation that would be incurred; however this requires further verification. On the other hand,  $\alpha$ -Al<sub>2</sub>O<sub>3</sub> did not suffer from this problem at the larger dimensions, with primary bursts being easily separated from subsequent reflections. Although the material had a higher overall attenuation, measured bursts showed significantly less distortion and (except for amplitude and energy) best-matched face-to-face signals in terms of AE features and frequency content.

Application of face angles increased attenuation for all materials and did not improve signal detectability even when mode conversion was known to occur. In the extreme 60-degree case, the measurable frequency range was almost always reduced. Similar deleterious affects were observed when pointed waveguides were tested.

Although use of waveguides in AE testing cannot be avoided, their implementation must be properly considered; dispersion, attenuation, mode conversion and/or waveguide reflections occurring within the waveguide will affect the signals being detected by the sensor. If possible, ends should be square and parallel (unless translational modes are expected in which no recommendations can be made) and materials should be selected depending on the transmission characteristics required for a particular monitoring task. If possible, specific designs should be tested prior to installation so that transmission characteristics can be verified.

### 5 ACKNOWLEDGEMENTS

The authors thank IMES Group for supplying the PCI2 board and software used for data acquisition.

### 6 REFERENCES

- [1] Graff, K. (1975) *Wave motion in elastic solids*, Clarendon Press, Oxford.
- [2] Redwood, M. (1960) *Mechanical Waveguides*, Pergamon Press, London.
- [3] Meeker, T.R., and Meitzler (1964) "Guided Wave Propagation in Elongated Cylinders and Plates" in Physical Acoustics, Vol 1., Part A, Academic Press Inc., pp112-169.
- [4] Cheeke, J.D.N. (2002) *Fundamentals and Applications of Ultrasonic Waves*, CRC Press, Boca Raton.
- [5] Beattie, A. G. (1983). "Acoustic Emission, principles and instrumentation." Journal of Acoustic Emission 2(1): 95-127.
- [6] (2002) *LabVIEW and LabWindows Signal Processing Toolset User Manual, Part No. 32214C-01*, National Instruments Corp., Austin Texas.
- [7] Wood, B.R.A., T. C. Flynn, et al. (1991). "The use of waveguides in acoustic emission monitoring projects" Acoustics Australia 19(3): 87-89.
- [8] Dupont, *Delrin Design Guide – ModuleIII* (available: [www.dupont.com](http://www.dupont.com))

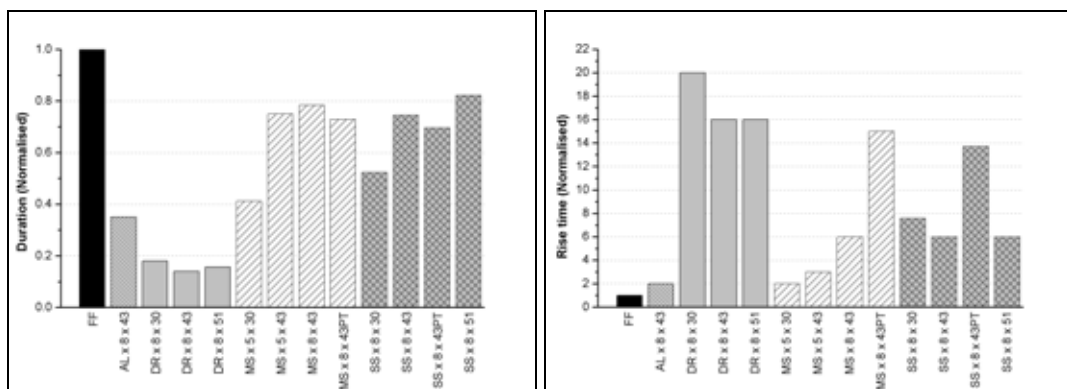


Figure 2: Normalised (a) duration and (b) rise time for all flat-faced waveguides

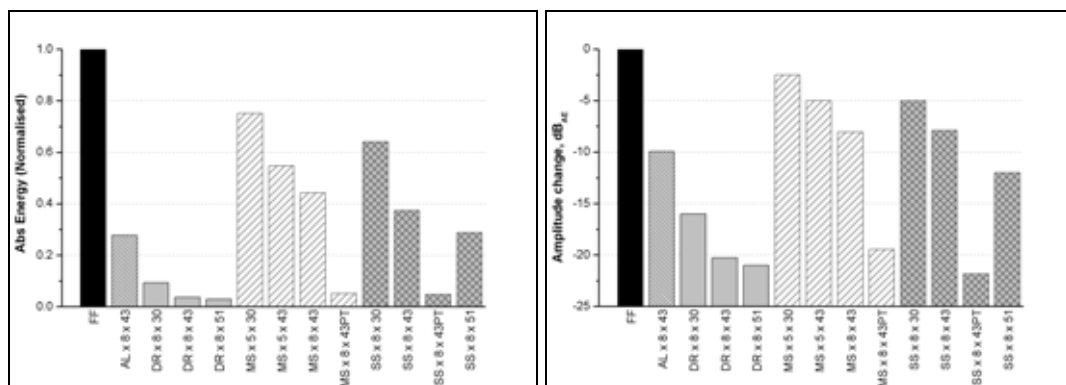
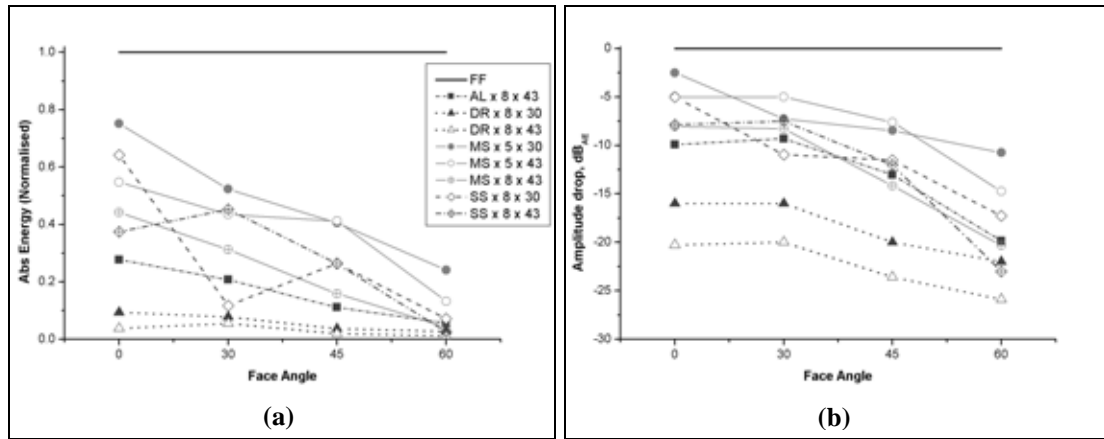
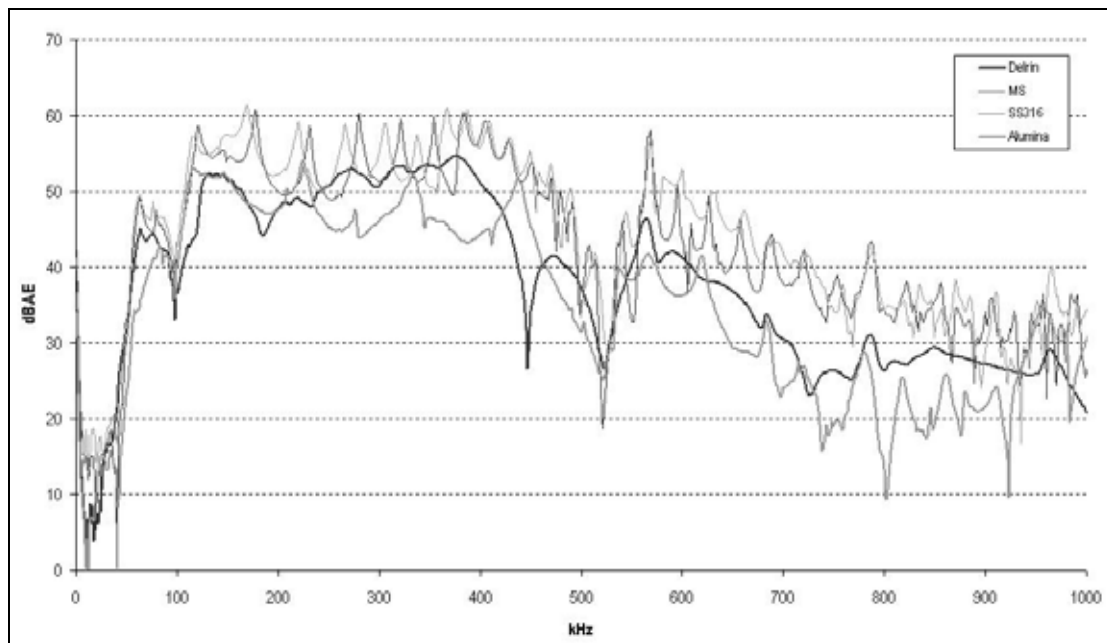


Figure 3: Normalised (a) energy and (b) amplitude for all flat-faced waveguides



**Figure 4:** (a) Normalised Energy and (b) Relative amplitude versus face angle for all sets of waveguides



**Figure 5:** Magnitude of Cross Power Spectrum for various materials – 8x43mm samples, flat faces

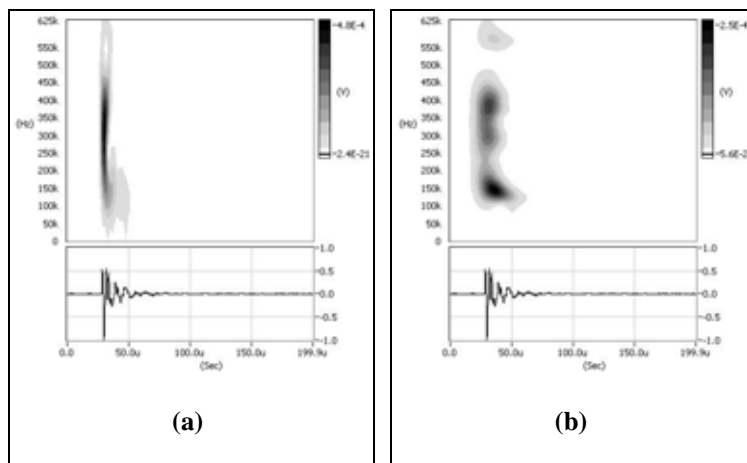
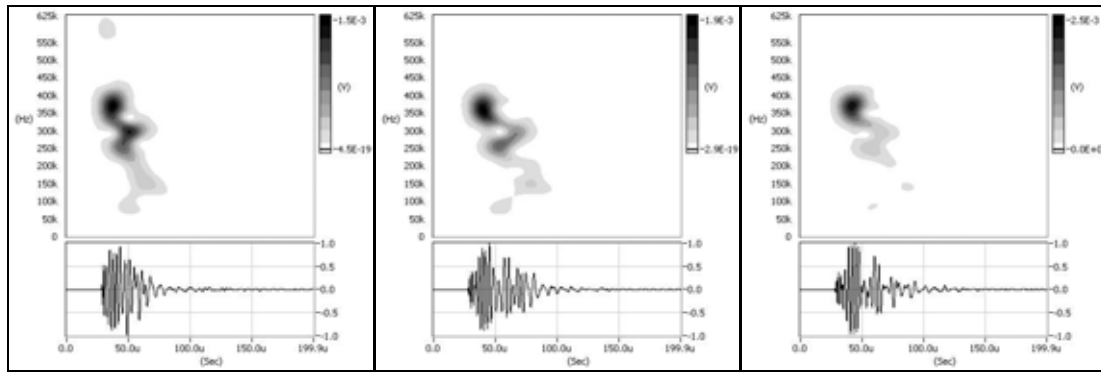
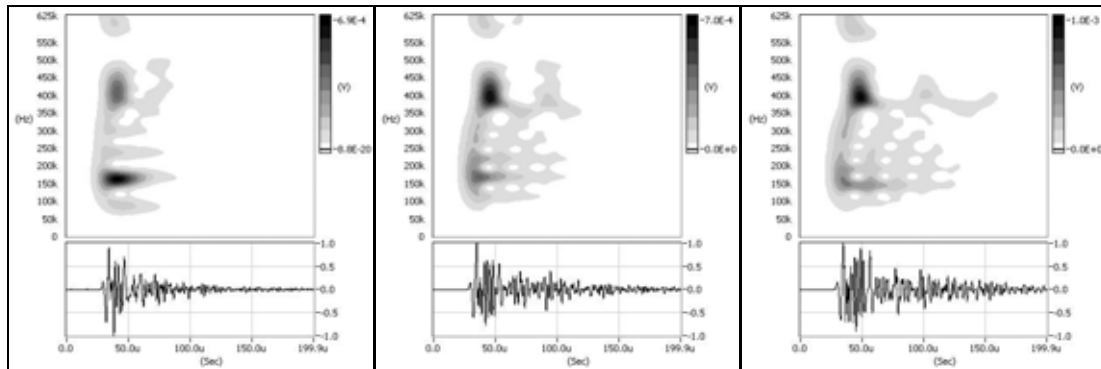


**Figure 6:** Face to Face STFT plots: (a) 128 and (b) 512 samples.



(a)



(b)

**Figure 7:** Effects of length on mode separation in (a) Delrin and (b) SS316 rods. Lengths are 30mm, 43mm and 51mm from left to right. (512 samples)

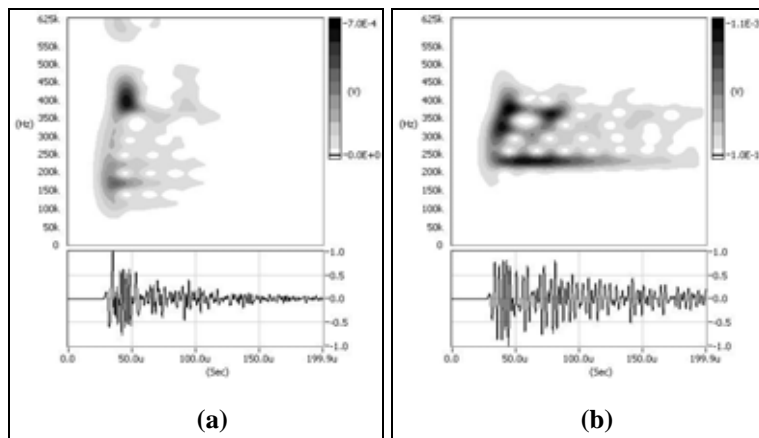


**Figure 8:** SSx8x43 (a) Flat faced and (b) Pointed waveguides. (512 samples)

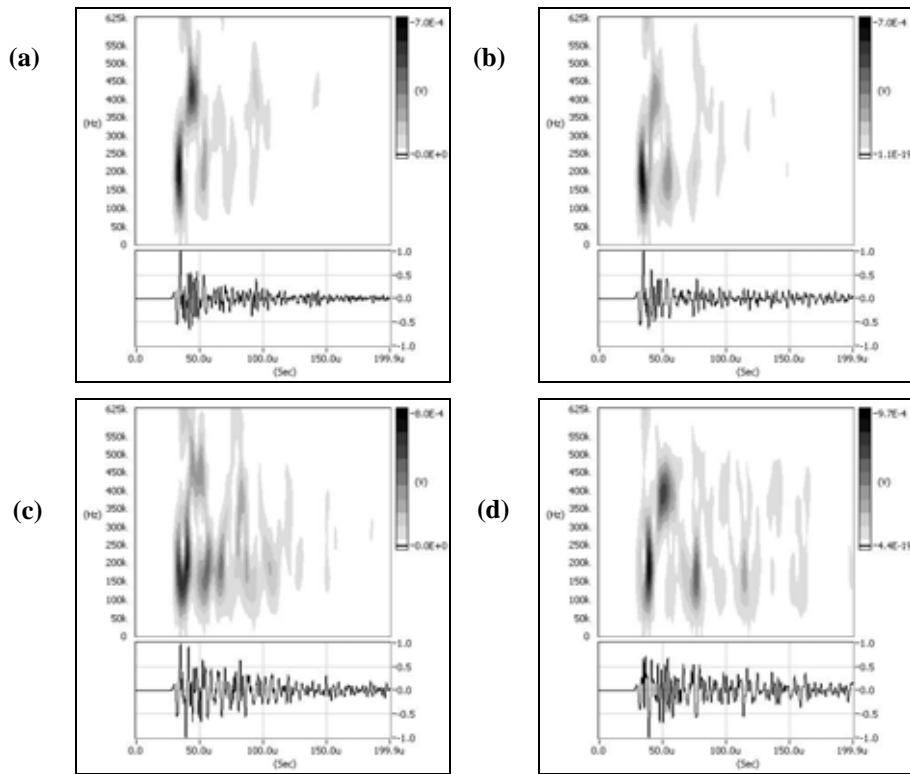


**Figure 9:** 8x43mm SS rods of different face angles: (a) 0 deg; (b) 30 deg; (c) 45 deg; and (d) 60 deg. (128 samples)

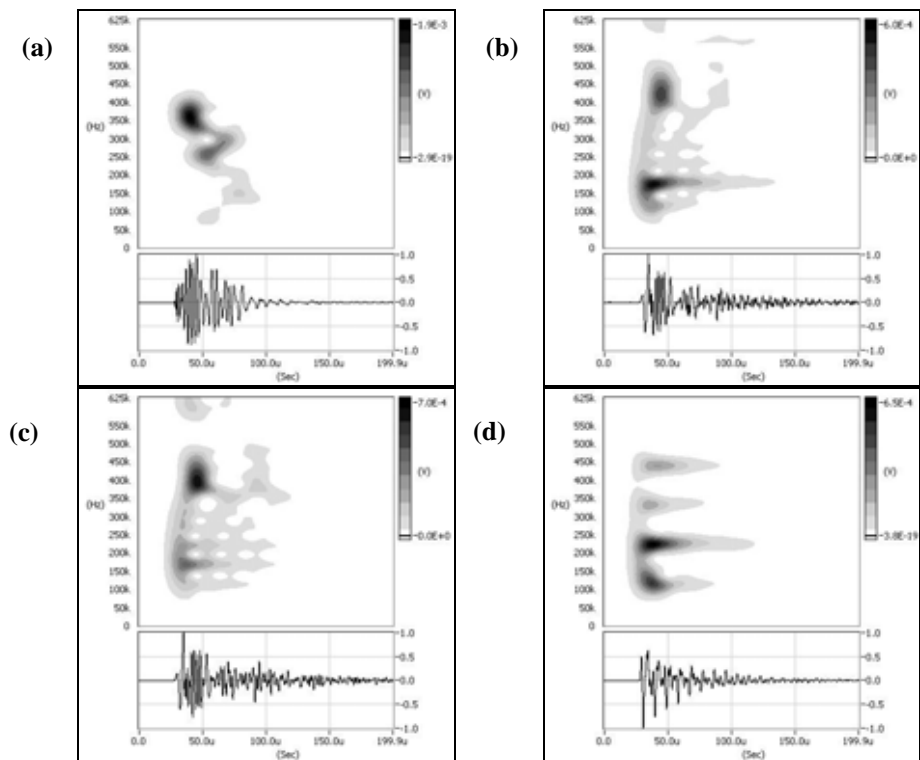


**Figure 10:** 8x43mm rods of different materials: (a) Delrin; (b) Mild Steel (c) SS316; and (d)  $\alpha$ -Al<sub>2</sub>O<sub>3</sub>. (128 samples)